Proceedings of the 17th World Congress
The International Federation of Automatic Control
Seoul, Korea, July 6-11, 2008

Energy saving Actuator Arrangements in an Actively Damped Engine Suspension System

Jörg Paschedag * **Guido Koch** * **Boris Lohmann** *

* *Institute of Automatic Control, Technische Universität München, D-85748 Garching near Munich, Germany (Tel: +49-89-28915664; e-mail: paschedag@tum.de, guido.koch@tum.de, lohmann@tum.de).*

Abstract: In this work, an active vibration control system is presented that reduces the transmission of engine induced vibrations to the chassis of a vehicle. In order to find system configurations which provide minimum energy consumption, six different configurations of actuator placement with two different actuator types are presented and analyzed regarding their power demands. Models for the test setup are derived and algebraic frequency dependent formulas for the calculation of average mechanical and electrical power consumption are deduced and discussed. The results of the analysis are compared to measurement data of an experimental test rig.

Keywords: Active vibration control, actuator location selection, energy saving, automotive, disturbance cancellation

1. INTRODUCTION

Especially in vehicles with combustion engines power consumption is a very important aspect particularly with regard to the ecological influence of emissions. On the other hand the customer demands on ride comfort and low-noise of vehicles are increasing continuously. The cancellation of disturbing machinery vibration is current concern of research and industrial development, Hansen and Snyder (1997), Howard (1999). One important application regarding this matter is the isolation of engine induced vibration in automobiles, Yu et al. (2000). Subject of this paper is a vibration attenuation system at the engine mounting with actively controlled force actuators. In car industry, sophisticated passive methods are already extensively applied for engine vibration isolation and semi active methods (e.g. with hydraulic mounts that vary stiffness and damping adaptively) are focus of current development, Braess and Seiffert (2003), Mitschke and Wallentowitz (2004). However, the possible benefits of active systems, like flexibility and high effectiveness, are rarely utilized. One of the main reasons for this is the potentially high power consumption of active systems. Aim of this paper is an estimation of the power demands to be expected and to determine an actuator arrangement which promises minimal energy demands for active damping.

For the analysis of power demands, an experimental setup is considered which is introduced in the following section. Furthermore, physical models for the dynamic behavior of the mechanical system and the actuators used are presented. The corresponding mathematical modelling is described in Section 3 as well as a derivation of frequency dependent formulas for the calculation of power demands. The results for the given application are shown and discussed in Section 4. The mechanical and electrical power demands are presented for the different actuator configurations and the requirements for energy recovery as well as the resulting benefits are discussed in particular.

2. MECHANICAL SETUP AND ACTUATORS

The mechanical system of interest is the mounting of an automobile engine on the car's chassis. The considered experimental setup is shown in Figure 1.

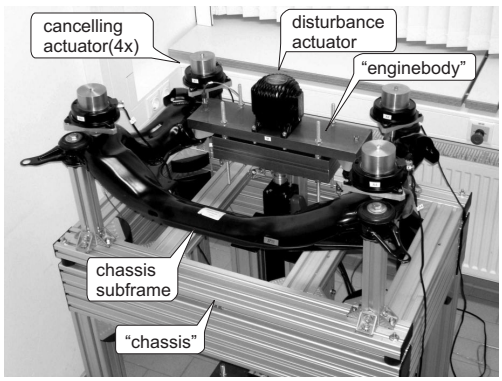

Fig. 1. Experimental setup

An actuator attached to a mass representing the engine body is used to excite the system mechanically. The mass is mounted at two points to a chassis subframe. The subframe itself is mounted at four points to a base framework which represents the car's chassis. The chassis subframe is a U-shaped, hollow steel body. The engine mass and the chassis subframe as well as the underlying "chassis" are connected by rubber mounts.

A finite element model of the test rig has been constructed (see Figure 2) in order to analyze the structural dynamics.

Using this model the main eigenmodes and -frequencies have been calculated and are used for the comparison of measurement data with simulations (Section 4).

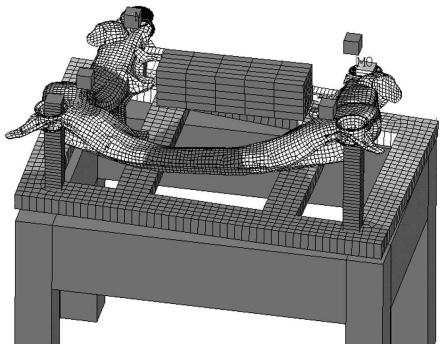

Fig. 2. Finite element model of the test rig

2.1 Rigid body model and actuation types for vibration control

The dynamic behavior of the rubber mounts in the test rig is assumed to be linear and the chassis subframe is considered to be rigid. Although nonlinearities of the rubber mounts are neglected, the linear modelling provides a useful basis for the presented estimation of power demands. Thus, the physical model shown in Figure 3 a) and b) can be derived for the setup. In the model, the spring and damping properties of the mounts are cumulated to the spring constants c_i and damping constants d_i.

In Figure 3 a) and b), two actuator principles are presented that are considered for the power analysis: The first one is that of a reaction mass actuator (Flint et al. (2000)) as installed on the experimental setup depicted in Figure 1. In this actuator type, the force actuator is built in between the mass to be attenuated and an additional mass m_A. These masses are connected via a spring and the friction forces between the masses can be approximated by a linear damper (Figure 3 a)). Thus a compensation of applied forces is accomplished by active dynamic absorption.

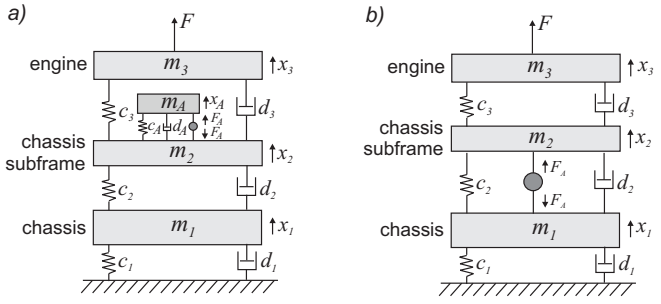

Fig. 3. Physical model of the engine mounting with a) force compensation, b) displacement compensation

For the second principle (Figure 3 b)), the force actuator is installed directly between two masses of the setup. This achieves a compensation of the displacement of the body. At the experimental setup shown in Figure 1, the actuator principle for force compensation is realized. A multichannel feedforward system (Kuo and Finn (1992), Kuo and Morgan (1996)) is used as control system. However, the displacement compensation will as well be subject to the following theoretical analysis.

2.2 Physical actuator models

The considered force actuators are of voice coil type, Miu (1993). The reasons for choosing this principle of force generation for the experimental setup are: Simple actuator structure, comparably low weight, uncomplicated electrical actuation as well as low friction and electrical counterforces with and without applied current. However, as will be shown in Section 3, no energy recovery is possible with the actuators used for this study.

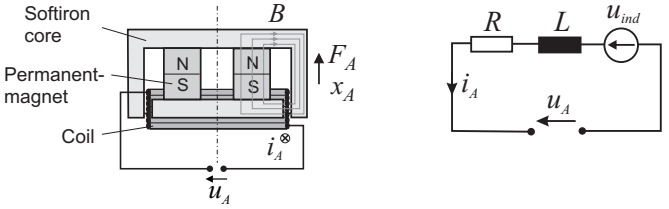

Fig. 4. Physical model of the force actuator

The actuators are physically modelled as shown in Figure 4 using the parameters explained in Table 1. The four real actuators can be replaced by a single one with four times the original values of mass as well as spring and damping constants (see Figure 3). The values of resistance R and inductance L are a quarter of the original ones. Voltages and other parameters remain unchanged.

Table 1. Parameters of the voice coil actuators

Parameter	Unit	Description
$c_A = 4.9 \cdot 10^4$	[N/m]	Spring constant
$d_A = 20$	[Ns/m]	Damping constant
$m_A = 2.56$	[kg]	Absorber mass
$R = 3.5$	[Ohm]	Coil resistance
$L = 1.2 \cdot 10^{-3}$	[H]	Coil inductivity
$N = 15$	[-]	Number of coil windings in the gap
$l = 0.245$	[m]	Coil perimeter
$B = 1.3$	[T]	Magnetic flux density

2.3 Actuator configurations

With the two different kinds of actuator principles applied to the basic three-body model in Figure 3, six configurations of actuator placement are possible. Figure 5 illustrates them schematically together with the shortcuts used in the following text. To maintain comparability of the configurations, the replacement of four real actuators by one in the model has been done as well for configurations *m3A* and *m23*. For active damping of the chassis subframe in these configurations two actuators would be sufficient. However, four actuators in parallel require half the electrical power for the same force generation as two actuators since actuator voltage and current are both proportional to the actuator force

It can be presumed that the configuration *m3A* is disadvantageous regarding energy demands: Since there are no intermediate passive damping elements, the actuators have to compensate for the complete accelerating forces at the engine body.

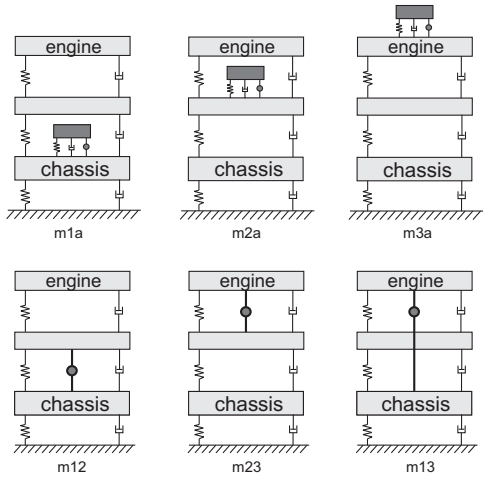

Fig. 5. Possible actuator configurations

3. MATHEMATICAL MODELING AND DERIVATION OF POWER DEMANDS

For a thorough analysis of the different actuator arrangements, mathematical models of the corresponding overall setups are needed. The modeling of the mechanical part can be done by applying Newton's second law. The electromechanical force actuator model of Figure 4 is connected by the Lorentz force $F_A(t)$ and the back emf $v_{emf}(t)$. Exemplary, the resulting set of equations for the configuration depicted in Figure 3 a) is:

Mechanical part:

$$\begin{aligned}
m_1\ddot{x}_1(t) &= -c_1x_1(t) - d_1\dot{x}_1(t) + c_2\left(x_2(t) - x_1(t)\right) \\
&\quad + d_2\left(\dot{x}_2(t) - \dot{x}_1(t)\right), \\
m_2\ddot{x}_2(t) &= -c_2\left(x_2(t) - x_1(t)\right) - d_2\left(\dot{x}_2(t) - \dot{x}_1(t)\right) \\
&\quad + c_3\left(x_3(t) - x_2(t)\right) + d_3\left(\dot{x}_3(t) - \dot{x}_2(t)\right) \\
&\quad + c_A\left(x_A(t) - x_2(t)\right) + d_A\left(\dot{x}_A(t) - \dot{x}_2(t)\right) - F_A(t), \\
m_3\ddot{x}_3(t) &= -c_3\left(x_3(t) - x_2(t)\right) - d_3\left(\dot{x}_3(t) - \dot{x}_2(t)\right) + F(t), \\
m_A\ddot{x}_A(t) &= -c_A\left(x_A(t) - x_2(t)\right) - d_A\left(\dot{x}_A(t) - \dot{x}_2(t)\right) + F_A(t).
\end{aligned}$$

Electrical part:

$$u_A(t) = L\frac{di_A(t)}{dt} + Ri_A(t) + u_{ind}(t)\ . \tag{1}$$

Connecting equations:

$$\begin{aligned}
F_A(t) &= BNl\ i_A(t)\ , \\
u_{ind}(t) &= BNl\left(\dot{x}_A(t) - \dot{x}_2(t)\right)\ .
\end{aligned} \tag{2}$$

For further analysis of the system, the describing equations are transformed into the Laplace domain. Initial values are set to zero.

An estimation of power demands is derived by assuming a complete vibration cancellation [1] for the body the actuator is mounted on. This assumption is equivalent to setting the displacement value of the body to zero in the Laplace domain. Thus, the order of the overall system is decreased. For a frequency related analysis, transfer functions from the excitation force $F(t)$ to the output variables of interest can be derived. Four transfer functions are needed in particular for the following estimation of power demands:

$$\begin{aligned}
G_{F_A}(s)\ &: F(s)\ \rightarrow\ \text{actuator force } F_A(s), \\
G_{v_A}(s)\ &: F(s)\ \rightarrow\ \text{actuator velocity } \dot{x}_A(s), \\
G_{u_A}(s)\ &: F(s)\ \rightarrow\ \text{actuator input voltage } v_{in}(s), \\
G_{i_A}(s)\ &: F(s)\ \rightarrow\ \text{actuator coil current } i(s).
\end{aligned} \tag{3}$$

The instantaneous mechanical power consumption is calculated by

$$P_{mech}(t) = F_A(t)\cdot\left(\dot{x}_A(t) - \dot{x}_2(t)\right)\ , \quad \dot{x}_2(t) = 0 \tag{4}$$

and the instantaneous electrical power consumption by

$$P_{el}(t) = u_A(t)\cdot i_A(t)\ . \tag{5}$$

Typically, the major part of the engine induced vibration is harmonic, Mitschke and Wallentowitz (2004). For one harmonic component $F(t) = |F|\cos(\omega t)$ of the excitation signal, the required electrical power for instance results from inserting the frequency responses (3) into (5):

$$P_{el}(t) = Re\left\{G_{u_A}(j\omega)|F|e^{j\omega t}\right\}\cdot Re\left\{G_{i_A}(j\omega)|F|e^{j\omega t}\right\} \tag{6}$$

By defining

$$\delta_{ui} = \angle G_{u_A}(j\omega) - \angle G_{i_A}(j\omega) \tag{7}$$

and transforming the received expression

$$\begin{aligned}
P_{el}(t) &= |F|^2\cdot Re\left\{|G_{u_A}(j\omega)|e^{j\angle G_{u_A}(j\omega)}e^{j\omega t}\right\} \\
&\quad \cdot Re\left\{|G_{i_A}(j\omega)|e^{j\angle G_{i_A}(j\omega)}e^{j\omega t}\right\} \\
&= |F|^2\cdot|G_{u_A}(j\omega)|\cdot\cos(\omega t + \angle G_{u_A}(j\omega))\cdot|G_{i_A}(j\omega)| \\
&\quad \cdot\cos(\omega t + \angle G_{i_A}(j\omega)) \\
&= \frac{1}{2}\ |F|^2\cdot|G_{u_A}(j\omega)|\cdot|G_{i_A}(j\omega)| \\
&\quad \cdot\left[\cos(2\omega t + \angle G_{u_A}(j\omega) + \angle G_{i_A}(j\omega)) + \cos(\delta_{ui})\right]
\end{aligned} \tag{8}$$

it becomes obvious, that the electrical power is a superposition of a constant value and a harmonic signal with a frequency twice as high as that of the original excitation signal $F(t)$. The mean value of the power consumption can be calculated by

$$\begin{aligned}
\bar{P}_{el} &= \frac{1}{T}\int_{t=0}^{T} P_{el}(t)dt \\
&= \frac{1}{2}\ |F|^2\cdot|G_{u_A}(j\omega)|\cdot|G_{i_A}(j\omega)|\cdot\cos(\delta_{ui})\ ,
\end{aligned} \tag{9}$$

where T is the fundamental period of the vibration.

This derivation can be performed in the same way for the average mechanical power. If the phase angle is defined as

$$\delta_{Fv}(\omega) = \angle G_{F_A}(j\omega) - \angle G_{v_A}(j\omega)\ , \tag{10}$$

for the average mechanical power follows

$$\begin{aligned}
\bar{P}_{mech} &= \frac{1}{T}\int_{t=0}^{T} P_{mech}(t)\,dt \\
&= \frac{1}{2}\ |F|^2\cdot|G_{F_A}(j\omega)|\cdot|G_{v_A}(j\omega)|\cdot\cos(\delta_{Fv})\ .
\end{aligned} \tag{11}$$

[1] In practice, a nearly perfect suppression can be achieved by feedforward algorithms. These work highly effective over the complete frequency range of interest (Widrow and Hoff (1960), Nelson and Elliott (1994), Kuo and Morgan (1996)).

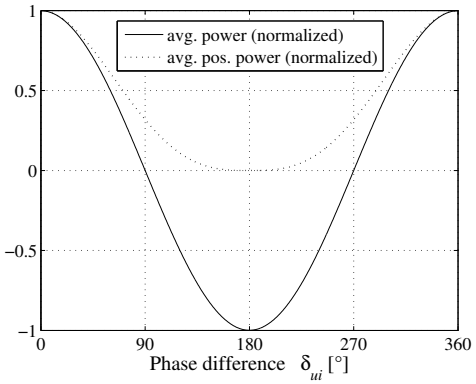

Fig. 6. $\bar{P}_{el}$ and $\bar{P}^{+}_{el}$ (and $\bar{P}_{mech}$, $\bar{P}^{+}_{mech}$ respectively), normalized to their common maximum value

It must be mentioned, that in practical application eq. (9) is in general only valid, if the phase difference between input voltage and current is

$$\delta_{ui}(\omega) = k \cdot 2\pi,\ k \in \mathbb{Z}\ . \tag{12}$$

Otherwise it must be distinguished whether power supplies with or without energy recovery are used. Energy recovery systems supply energy while $P_{el}(t)$ is positive and recover energy when $P_{el}(t)$ is negative. Without energy recovery, no energy is fed back from the system. In that case, the actual power demands are given by the average positive power which is calculated by

$$\bar{P}^{+}_{el} = \frac{1}{T}\int_{t=0}^{T} P^{+}_{el}(t)dt \tag{13}$$

$$P^{+}_{el}(t) = \begin{cases} P_{el}(t) & \text{if} \quad P_{el}(t) > 0 \\ 0 & \text{else} \end{cases}\ . \tag{14}$$

Equality of the powers $\bar{P}_{el} = \bar{P}^{+}_{el}$ only holds true if eq. (12) is satisfied. If the phase difference differs from eq. (12) significantly, considerably less power is needed if energy recovery is used. Figure 6 shows the relation between the phase difference δ_{ui} and $\bar{P}_{el}$ as well as $\bar{P}^{+}_{el}$ (naturally, the depicted characteristic is 2π-periodic).

In order to achieve a more general analysis of the power demands, the consideration presented for the electrical power consumption can be done for the mechanical power analogously. In that case, for the operation with energy recovery an appropriate power conversion from electrical to mechanical power is necessary. Thus, ideally the actuator voltage $u_A(t)$ would be proportional to the velocity $v_A(t)$ and the current $i_A(t)$ proportional to the force $F_A(t)$, Okada and Harada (1996). Only in this case the discussed results can be derived for the mechanical power demands as well using the phase angle δ_{Fv}. Then the ratio of $\bar{P}_{el}$ and $\bar{P}^{+}_{el}$ shown in Figure 6 would be the same for the mechanical powers $\bar{P}_{mech}$ and $\bar{P}^{+}_{mech}$.

Especially for the voice coil actuators used here, the phase difference is mainly given by the phase characteristic of the electrical system described by eq. (1). For an estimation of the shape of the characteristic, the effect of the back emf $v_{emf}(t)$ can be neglected. The cut-off frequency of the remaining first order system is determined by the quotient R/L. In the given case the cut-off frequency equals approx. 500 Hz. Since the frequency of the signal to be cancelled will normally not exceed 300 Hz, the resulting phase differences $\delta_{ui}(\omega)$ and $\delta_{Fv}(\omega)$ respectively remain small in the relevant frequency range. The maximum phase difference at 300 Hz is about 30°. As a consequence, for the given case the power demands will approximately be the same for power electronics with and without energy recovery (see Figure 6).

4. FREQUENCY DEPENDENT POWER DEMANDS AND EVALUATION

Following from the previous section, the average mechanical and electrical power demands can be described by $\bar{P}_{mech} = K_{mech}(\omega) \cdot |F|^2$ and $\bar{P}_{el} = K_{el}(\omega) \cdot |F|^2$ with

$$K_{mech}(\omega) = \frac{1}{2}|G_{F_A}(j\omega)| \cdot |G_{v_A}(j\omega)| \cdot \cos(\delta_{Fv}(\omega))\ ,$$
$$K_{el}(\omega) = \frac{1}{2}|G_{u_A}(j\omega)| \cdot |G_{i_A}(j\omega)| \cdot \cos(\delta_{ui}(\omega))\ . \tag{15}$$

These frequency dependent quantities represent the power needed to compensate the engine vibration transferred to the chassis completely for a given squared excitation force $|F|^2(\omega)$. Therefore they represent inverse efficiency spectra of the system including passive damping.

In the case of harmonic excitation, the total power demands are given by

$$\bar{P}^{res}_{mech} = \int_{\omega=\omega_{min}}^{\omega_{max}} \bar{P}_{mech}(\omega)\, d\omega\ , \tag{16}$$

$$\bar{P}^{res}_{el} = \int_{\omega=\omega_{min}}^{\omega_{max}} \bar{P}_{el}(\omega)\, d\omega\ . \tag{17}$$

4.1 Mechanical Power Demands

In Figure 7 the characteristic $K_{mech}(\omega)$ is presented for the six different actuator configurations of Figure 5. The characteristic is scaled to $K_{mech}[\text{dB}] = 10 \cdot \log_{10}(K_{mech})$. The plot of configuration *m13* is visualized for values up to about 50 Hz only since $K_{mech}(\omega)$ is negative for higher frequencies. This indicates a gain of mechanical energy. As shown in Figure 8 (linearly scaled), the absolute value of the negative power is significant in the frequency range between 60 and 70 Hz where an eigenmode of the chassis subframe emerges. The voice coil actuators are not able to utilize this effect to gain energy but other types of force actuators would be.

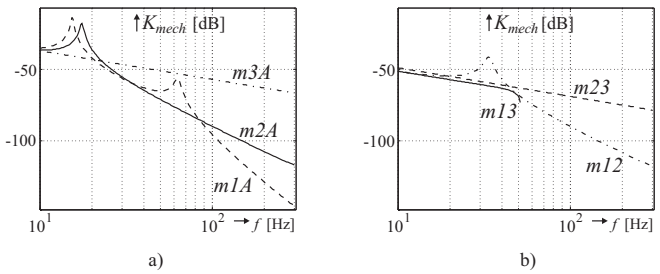

Fig. 7. Spectra of the average mechanical power demands for a) force compensation and b) displacement compensation

In Figure 9 the products of the amplitude characteristics $|G_{F_A}(j\omega)|$ and $|G_{v_A}(j\omega)|$ as well as the difference of the

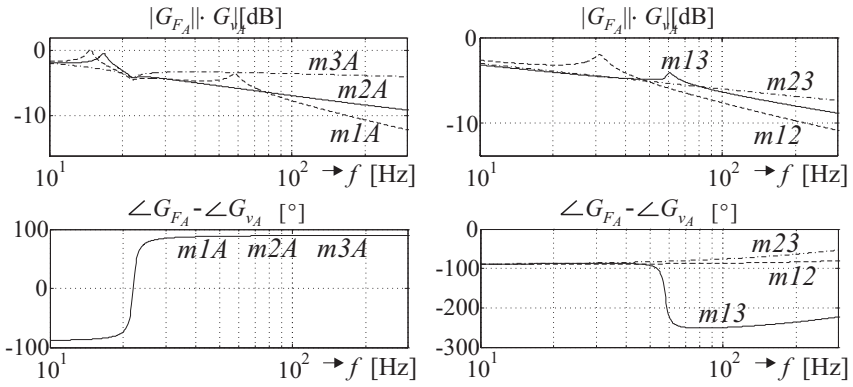

Fig. 9. Amplitude products and phase differences of $G_{F_A}(t)$ and $G_{v_A}(t)$

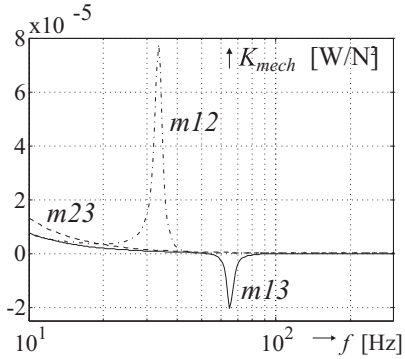

Fig. 8. Power demands of displacement compensation (linearly scaled)

corresponding phase characteristics are displayed. These characteristics show in connection with eq. (11) and Figure 6 the difference of power demands for a system with and without energy recovery.

The phase difference in Figure 9 is $\delta_{Fv}(\omega) \approx (2k+1) \cdot 90°$, $k \in \mathbb{Z}$ for force compensation and displacement compensation over most of the relevant frequency range. The reason for this is in the case of displacement compensation that the force $F_A(t)$ is mainly determined by the force of the spring elements (e. g. c_3 at the setup *m23*). This force is proportional to the spring deflection (e. g. $x_3 - x_2$ for *m23*). As a result a phase difference of $\delta_{Fv}(\omega) \approx 90°$ for the configurations *m12* and *m23* over the considered frequency range occurs.

Because of the transition from undercritical to overcritical excitation frequencies at approx. 60 Hz, a phase difference of about 270° occurs at the configuration *m13* for higher frequencies. For all displacement compensation configurations the influence of velocity proportional damping forces increases with higher frequencies and their phase differences deviate from the values $-90°$ and $-270°$ respectively in the high frequency range.

The dynamical behavior of the configurations with force compensation is similar in the low frequency range: The force $F_A(t)$ is mainly determined by the spring elements which cause a phase shift by $-90°$. For frequencies above the resonance frequency, the force $F_A(t)$ is approximately proportional to the sum F_{res} of the forces generated by the actuators including the actuators' spring and damper elements. Accordingly the force $F_A(t)$ generated by the voice coil actuators is proportional to $\ddot{x}_A(t)$. Since $\ddot{x}_A(t)$ is the derivative of the actuator velocity $v_A(t)$, a phase difference of $\delta_{Fv} = 90°$ results.

In summary it can be stated that with the characteristics of δ_{Fv} shown in Figure 6, a system with energy recovery can potentially be considerably more efficient for the given application than a system without energy recovery. This is especially the case for configuration *m13*.

4.2 Electrical Power Demands

Figure 10 shows the characteristics $K_{el}(\omega)$ of the electrical power consumption. For the application in a real car, the actual power demands are not easy to determine. Besides the depicted characteristics they depend on the excitation force magnitude $|F|$ which is strongly influenced by the considered engine type and its load profile. Nevertheless, for a simplified analysis the integral of $K_{el}(\omega)$ over the relevant frequency range can be used as a measure for the overall energy demands. In addition to that, the peak value of $K_{el}(\omega)$ indicates the maximum necessary load limits of the actuators. Taking into account these quality criteria and the logarithmic scaling of Figure 10, it shows that the configuration *m2A* is presumably the best solution regarding electrical power demands. Second-best is the arrangement *m1A*. Especially at frequencies of approx.

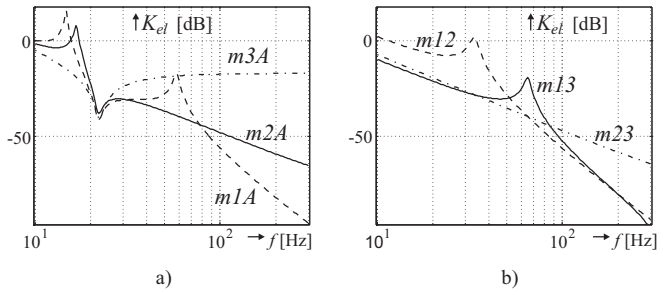

Fig. 10. Spectra of the average electrical power demands for a) force compensation and b) displacement compensation

60 Hz, $K_{el}(\omega)$ is much higher for *m1A* than for *m2A* because the chassis subframe m_2 is not damped by the active vibration control system and therefore causes a large force on the body m_1 at its resonance frequency. In Figure 11, the calculated results are compared to measurement data from the experimental setup. Here it can be seen

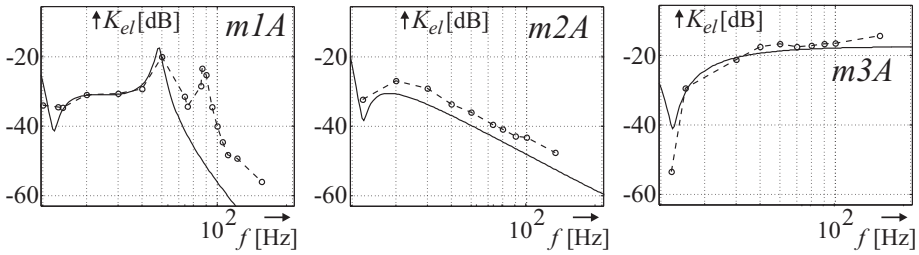

Fig. 11. Comparison of theoretical results with measurement data of the test rig

that for *m1A*, besides the mode at about 60 Hz, another mode of the chassis subframe at about 90 Hz is excited that is not reproduced by the simple three body model of the engine mounting (Figure 3). This has been verified using the finite element model of the mechanical test rig structure (Figure 2). Table 2 shows the total electrical power demands for the different actuator configurations with respect to the type of engine force. In a combustion engine, force components generated by the combustion itself are nearly constant while the inert forces of the engine increase with the square of the engine speed ω_e. Consequently, the required power differs for each setting but nevertheless it can be seen that configuration *m2A* requires least power for active damping.

Table 2. Total power demand, normalized on the smallest value (*m2A*)

Configuration	$\bar{P}_{el}^{res}$ for $\lvert F\rvert = const$	$\bar{P}_{el}^{res}$ for $\lvert F\rvert \sim \omega_e^2$
m1A	5.6	8.0
m2A	1.0	1.0
m3A	224	3800
m12	372	159
m23	3.0	1.7
m13	6.7	8.1

5. CONCLUSION

In the efficiency analysis presented in this paper the frequency dependent power demands of different actuator configurations for the active damping of vehicle engine vibrations have been compared. The spectra of the ratio of the required mechanical and electrical power and the squared amplitude of the engine force $|F|^2(\omega)$ have been derived.

Two different operating principles of the actuator setups have been distinguished: Displacement compensation, which offers a higher efficiency regarding the mechanical power demands, and force compensation, which has proven to be superior regarding electrical power demands due to the special kind of actuator considered here (active dynamic absorber).

The required electrical power is significantly lower if an actuator concept with energy recovery is used. Especially for the actuator configuration *m13* it is possible to gain energy in time average. In order to benefit from these lower power demands, actuators as well as power electronics must be used that can recover energy during operation in the test setup. This is not the case for the voice-coil actuators used in the experiments of this study. Even if the power electronics could handle energy recovery, only a marginal amount of power saving could be reached.

In this study only translational vibrations have been considered for the power demands while at the test rig and in particular in a vehicle with a combustion engine, rotational modes of the chassis subframe are excited as well. The finite element analysis however shows that the system has a similar characteristic behavior for the rotational modes as for the translational modes, e.g. the main eigenfrequencies occur in the same frequency range.

Especially for the application in a vehicle, minimum energy consumption is a very important aspect. With appropriate actuators the discussed concepts of this study could be applied with an effective energy recovery. As a consequence, the applicability of present methods for active vibration control would be considerably improved.

REFERENCES

H.-H. Braess and U. Seiffert. *Vieweg Handbuch Kraftfahrzeugtechnik*. Vieweg, Wiesbaden, 2003.

E. Flint, M. E. Evert, E. Anderson, and P. Flannery. Active/passive counter-force vibration control and isolation systems. In *Proceedings of the IEEE 2000 Aerospace Conference*, page Paper No. 432, 2000.

C. H. Hansen and S. D. Snyder. *Active Control of Noise and Vibration*. E & FN Spoon, London, 1997.

C. Q. Howard. *Active isolation of machinery vibration from flexible structures*. PhD dissertation, The University of Adelaide, 1999.

S. M. Kuo and B. Finn. A general multi-channel algorithm for 3-d active noise control systems. In *in Proc. Int. Cong. Recent Developments in Air- Structure-Borne Sound and Vibration*, pages 345–352, March 1992.

S. M. Kuo and D. R. Morgan. *Active Noise Control Systems*. John Wiley & Sons, New York, 1996.

M. Mitschke and H. Wallentowitz. *Dynamik der Kraftfahrzeuge*. Springer, Berlin, Heidelberg, New York, 2004.

D. K. Miu. *Mechatronics*. Springer-Verlag, New York, 1993.

P. A. Nelson and S. J. Elliott. *Active Control of Sound*. Academic Press, London, 1994.

Y. Okada and H. Harada. Regenerative control of active vibration damper and suspension systems. In *Proceedings of the 35th Conference on Decision and Control, Kobe, Japan*, pages 4715 – 4720, 1996.

B. Widrow and M. E. Hoff. Adaptive switching circuits. In *1960 IRE WESCON Convention Record, New York IRE*, pages 96–104, 1960.

Y. Yu, N. G. Naganathan, and R. V. Dukkipati. Review of automotive vehicle engine mounting systems. *Int. J. Vehicle Design*, 24(4):299–319, 2000.